Print ISSN: 0375-9237
Online ISSN: 2357-0350

EGYPTIAN JOURNAL OF BOTANY (EJBO)

In vitro, ex vivo, antiobesity activity and chemical profiling of *Euclea racemosa* subsp. *Schimperi* aqueous fraction

Hanan M. El-Tantawy

PUBLISHED BY
THE EGYPTIAN
BOTANICAL SOCIETY

In Vitro, *Ex Vivo*, Antiobesity Activity and Chemical Profiling of *Euclea racemosa* subsp. *schimperi* Aqueous Fraction

Hanan M. El-Tantawy
Medicinal and Aromatic Plants Department, Desert Research Center, Cairo, Egypt

Adipogenesis is linked to obesity through the proliferation and deposit of preadipocytes as adipose tissues occur at various sites in the body. This study investigated the effects of *Euclea racemosa* subsp. *schimperi* extracts *in vitro* on lipase enzymes to identify the most active fractions. Then, the bioactive fraction was injected *ex vivo* on the high-fat diet adipose tissue (HFD-AD). Afterward, the lipid profile, oxidant/antioxidant parameter, and lipid accumulation were measured inside the cells. Finally, LCMS/MS for this fraction was performed. The aqueous fraction exhibited a stronger inhibitory effect on lipase enzymes with an IC_{50} of 18.15±1.24 µg/ml compared to orlistat's (IC_{50} of 5.27±0.62 µg/ml). The aqueous fraction and methylsulfonyl-methane (MSM) were administered to HFD-AD cells at concentrations of (0.529±0.025 and 0.093±0.02 µg/ml), respectively. There was no significant difference ($p > 0.05$) between the effects of MSM and the aqueous fraction on controlling lipids profile parameters (triglycerides (TG), cholesterol (C), low density lipoprotein-cholesterol (LDL-C), and high density lipoprotein-cholesterol (HDL-C)). Furthermore, the aqueous Fr. reduced lipid accumulation, malondialdehyde (MAD), and nitric acid (NO) activity compared to untreated cells with a non-significant difference compared to the MSM ($p > 0.05$). Additionally, the aqueous Fr. showed an increase in total antioxidant capacity (TAC) and catalase (CAT) activity significantly compared to the MSM ($p<0.05$). In conclusion, The aqueous Fr. improved lipid accumulation, lipid profile, oxidative stress, and antioxidant effects. These activities are attributed to various compounds identified by LC MS/MS.

Keywords: *Euclea racemosa* subsp. *schimperi*, lipases inhibition, high-fat diet adipose tissue, oil red o staining, obesity

ARTICLE HISTORY
Submitted: August 05, 2024
Accepted: November 12, 2024

CORRESPONDANCE TO
Hanan M. El-Tantawy,
Medicinal and Aromatic Plants Department,
Desert Research Center, Cairo, Egypt
Email: hanantantawy@gmail.com
DOI: 10.21608/ejbo.2024.309874.2954

EDITED BY: M. Madany

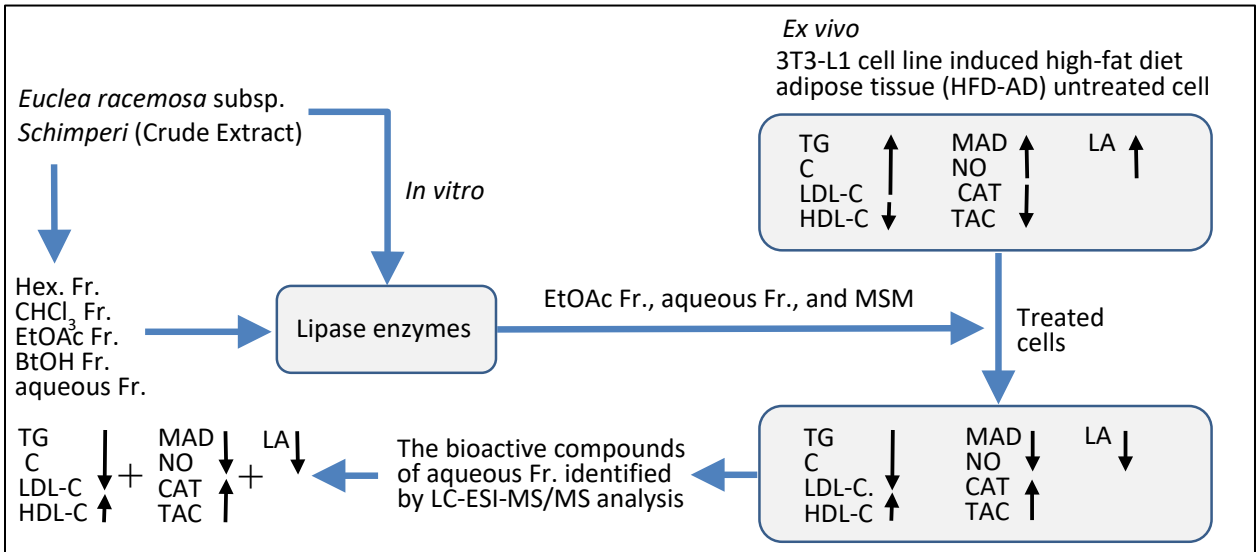

Graphical Abstract: Triglycerides (TG), cholesterol (C), low density lipoprotein-cholesterol (LDL-C), high density lipoprotein-cholesterol (HDL-C), malondialdehyde (MAD), nitric acid (NO), catalase (CAT), total antioxidant activity (TAC) and lipid accumulation (LA).

INTRODUCTION

A high-fat diet (HFD) can lead to the accumulation of excess body fat, which is linked to obesity. Diet-related obesity has been attributed to increased oxidative stress and liver inflammation (Kim et al., 2019). Obesity is a complex disorder caused by the interaction of numerous types of genetic, nutritional, lifestyle, and environmental factors (Karri et al., 2019). It is a risk factor for metabolic syndrome leading to dyslipidemia, which is a lipid abnormality that includes high levels of triglycerides (TG) or/and cholesterol (C) due to high levels of low density lipoprotein-cholesterol (LDL-C, bad cholesterol) and low levels of high density lipoprotein-cholesterol (HDL-C, good cholesterol), which causes liver failure, cardiovascular complications, acute pancreatitis, hypertension, and pro-inflammatory (Khatua et al., 2017; Al-Rawi, 2019). Lipid abnormalities contribute to elevated oxidative stress via several biochemical

processes that can impair bodily functions, promote the development of obesity-related metabolic syndrome by causing an excess of reactive oxygen species (ROS), induce an imbalance in the amount of energy intake and expenditure (Manna, 2015) and encourage the deposition of adipose tissue including preadipocyte proliferation, adipocyte differentiation, and growth (Čolak et al., 2022). Throughout the stages of obesity, adipose tissue can expand by an increase in adipocyte size (hypertrophy) or an increase in adipocyte number through the differentiation of new adipocytes (hyperplasia) or a combination of hypertrophy and hyperplasia tissue at various sites in the body as depots or subcutaneous fat and has a significant impact on the body's overall metabolism, a process known as adipogenesis (Jakab et al., 2021). Adiposity leads to lipo-inflammation and increased oxidative biomarkers [malondialdehyde (MDA) level and nitric oxide (NO)] and a decrease in the activity of antioxidant defenses as catalase enzyme activity (CAT) and total antioxidant activity (TAC) leading to various abnormalities (Croft et al., 2023). Consequently, reducing oxidative stress and adipose tissue may be useful in preventing the harmful effects of obesity; lowering amounts of stored and circulated lipids (TG and C) and LDL-C were critical for managing obesity (Čolak and Pap, 2202). Alterations in diet and increased exercise can help control obesity, but these methods take a long time to become effective, so many people prefer surgical interventions and therapeutic agents to get the same results in a short time (Bhardwaj et al., 2021). There are numerous drugs on the market that can aid in weight reduction by decreasing food intake, boosting energy expenditure during physical activity, and limiting intestinal fat absorption. One approach involves the reversible inhibition of pancreatic lipase enzymes, which hinders the breakdown of triglycerides into absorbable monoglycerols and free fatty acids. Orlistat is a prime example of a drug that operates through this mechanism (Mahboob et al., 2023; Abdel Raoof, 2022). Methylsulfonylmethane (MSM) reduces HFD, anti-inflammatory, antioxidant properties improve lipid profiles that help to prevent diseases associated with obesity (Miller et al., 2021). Several adverse health effects are related to these medications, such as hypertension, depression, and cardio metabolic anxiety, diarrhea, abdominal pain, deficiency in fat-soluble vitamins, incontinence, and frequent bowel movements (Khatua et al., 2017). For this reason, a wide range of natural products have been investigated for treating obesity. Given that different natural anti-obesity medicines work through various mechanisms without side effects (Čolak and Pap, 2022). Natural plants contain a wide variety of medicinal pharmaceuticals due to their ability to minimize adipose tissue mass through inhibiting adipogenesis (Abdel-Sattar et al., 2014). For this *in vitro* investigation, the 3T3-L1 cell line was selected because it is widely utilized in research on obesity and has a reputation for being the most realistic in simulating an obese state by the injection of HFD, which initiates differentiation and adipogenesis (Mubtasim and Gollahon, 2023). Ebenaceae family contains plants such as *Diospyros kaki*, which improves hyperglycemia, dyslipidemia, and liver fat accumulation in type 2 diabetics (Jung et al., 2012), *Diospyros lotus* reduced body weight gain with reduced TG, total cholesterol, and low-density lipoprotein cholesterol (Kim et al., 2019), and *Euclea natalensis* prevented lipid peroxidation (Batia et al., 2024). *Euclea racemosa* subsp. *schimperi* is used for multiple purposes as food (fruit) and traditional medicine (for the treatment of cancer, wounds, toothaches, malaria, abdominal pain and inflammation) (Asres et al., 2006). The chemical constituents in the plant are coumarins, triterpenes, alkaloids, sterols, flavonoids, naphthoquinones, and cardiac glycosides. Because of this, the plant engages in a variety of biological activities (Taye et al., 2023). In previous studies, flavonol isolated from the plant leaves (quercetrin, myricitrin, rutin, and myricetin-3-O-arabinopyranoside) have significant antioxidant activity (Asres et al., 2006). Therefore, this study intends to investigate the effects of *E. racemosa* subsp. *schimperi* aerial parts methanolic extract subsequently its fraction *in vitro* experiment, such as enzymatic inhibition of lipase enzymes. The most active fractions that inhibited lipase enzyme were used in treatment of HFD adipocytes and markers of oxidative stress, antioxidants, lipid profile were measured. The results were confirmed by oil-red staining-based lipid accumulation. LC-MS/MS proceeded to the most potent fraction.

MATERIAL AND METHODS

Plant Material

The aerial parts of plant utilized in this study were obtained from the Elba Mountain region and documented as *Euclea racemosa* subsp. *schimperi* (A.DC.) F. White, Ebenaceae family by Dr. Mahmoud Ali, Associate Professor of Plant Ecology, Desert Research Center, the specimens are recorded under number (CAIH-1254-R).

Extraction and Fractionation

Fresh aerial parts of the plant were air-dried and ground to powder. The powder (2.5 kg) of the plant was macerated with 80% ethanol at room temperature (1.5 × 4.5 L) for 48 hours. The extracts obtained were concentrated on the rotary evaporator under vacuum at 45 °C until dryness, producing 67.32 g of the total extract. The dried extract was evaluated for its effectiveness against the Lipase enzyme *in vitro*. Followed by bioguided fractionation by suspending the extract in 70% MeOH (600 mL) in a separating funnel and partitioning with n-hexane (Hex.), chloroform ($CHCl_3$), ethyl acetate (EtOAc.), butanol (BtOH), and distilled water, yielding five fractions (12 g, Hex. Fr.), (11.29 g, $CHCl_3$ Fr.), (8.93 g, EtOAc Fr.), (15.52 g, BtOH Fr.), and (19.30 g, aqueous Fr.). These fractions were subjected *in vitro* for their ability to inhibit lipase activity, to identify the most potent fractions for use HFD-AD cells.

Enzymatic Inhibitory Assay *In vitro*

The porcine pancreatic lipase II (PPL) was prepared according to Lewis and Liu, (2012). PPL type II (L-3126) was dissolved in 50 mM phosphate buffer pH 7 (1 mg/ml) and centrifuged at 12,000 x g for 5 minutes to eliminate any insoluble components. The concentration of enzyme stock was 0.1 mg/ml for each 1 mg of PPL solid powder diluted in 1 ml of buffer, and the solutions were kept at 20°C. *P*-nitrophenyl palmitate (*p*NPB, substrate): 2.5 mM pNPB was dissolved in 1% dimethylsulfoxide (DMSO), then diluted with 100 µl reaction buffer solution. In addition to, phosphate buffer pH 7 and the orlistat drug, all previous materials were purchased from Sigma. The ability of *E. r.* ssp. *Schimperi* extract to inhibit PPL was measured using the Lewis method with minor modifications reported by (Alias et al., 2017). The lipase inhibition assay was carried out by incubating the methanolic extract of the plant, followed by its different fractions (Hex, $CHCl_3$, EtOAc, BtOH, and aqueous) ranging in concentration from 0.25 to 500 µg/ml with PPL and pNPB (50 mM potassium phosphate buffer, pH 7.2, 0.5% Triton X-100) for 10 minutes in 96-well plates. All tests were run at 37 °C, and the presented data are the average of three replicates after subtracting blank values. Orlistat served as a standard inhibitor. DMSO was used as a negative control, and the activity was also examined with and without the inhibitor. Lipase activity was measured by tracking the hydrolysis of p-nitrophenyl butyrate to *p*-nitrophenol at 405 nm by using UV-transparent 96-well plates on an ELISA reader (BIO-TEK, Synergy HT, USA). One unit of activity was defined as the rate of reaction that creates 1 µmol of *p*-nitrophenol per minute at 37 °C. When PPL was incubated with the test compounds, the inhibition of the lipase activity was detected as a percentage decline in the activity. According to the following formula, the lipase inhibition (%) was calculated: Lipase inhibition (%) = 100 - [(B-b) / (A-a) x 100]. Where A is the activity without inhibitor, a is the negative control without inhibitor, B is the activity with inhibitor, and b is the negative control with inhibitor. IC_{50} value is calculated for the most potent plant extract that inhibits lipase by 50%. The IC_{50} value was calculated using GraphPad Prism Version 4.0 software (GraphPad Software Inc., San Diego, USA).

Cellular Model of Adipogenesis *Ex vivo*

The 3T3-L1 cell line was obtained from male Sprague-Dawley rats, which is a precursor cell line generated from mouse embryonic fibroblasts. At 37 °C in an incubator with 5% CO_2, the cells were cultured in Dulbecco's Modified Eagle Medium (DMEM) supplemented with 10% fetal bovine serum (FBS), 1% penicillin, and 1% streptomycin. All chemical compounds are used in this model from Gibco, Thermo Scientific, USA.

Establishing a Primary Culture of Adipocytes Using the 3T3-L1 Cell Line of Rats' **Induced HFD**

Primary cultures of adipocyte cells from rats are a valuable biological model for evaluating the mechanisms of adipocyte differentiation and adipogenesis linked to obesity and dysfunctional adipocytes in *ex vivo*. Preparation of primary culture of adipocytes from rats involves a series of steps, including isolation, processing, digestion, filtration, resuspension, and differentiation of adipose tissue cells, respectively, according to (Van and Roncari, 1977; Etesami et al., 2020). Adipose tissue was isolated from male Sprague-Dawley rats, aged 18–25 days and weighed 40–64 g after the aesthesia, kindly killed under sterile conditions, and it placed in a Petri dish containing 0.9% saline for the removal of the epididymal fat pad from the border of the epididymis. Adipose tissue samples were processed by placing them in a sterile flask containing a culture medium called Dulbecco's Modified Eagle Medium (DMEM, Gibco, Thermo Scientific, USA). To get rid of any blood or debris, the cells are washed three times with 10% fetal bovine serum (FBS). Following that, the tissues were cut into tiny pieces (1 to 2 mg) with a scalpel or sterile scissors. Subsequently, the cells were digested by 1 ml of enzymatic buffer solution (0.5% collagenase

solution in Hank's Balanced Salt Solution (HBSS), Gibco, Thermo Scientific, USA) to separate the adipocytes from the surrounding tissue, then incubated under stirring for 45–60 min at 37°C until the tissue appeared well-digested. After that, the cell suspension was filtered through a cell strainer to eliminate any remaining undigested tissue pieces and produce a single-cell suspension. centrifuged to the filtered suspension at a slow speed for 5 to 10 min, at 300 to 400 g. In the end, the cell pellet was kept, and the supernatant was thrown away. The adipocyte pellet was again suspended in a fresh culture medium that contained 1% antibiotics (penicillin-streptomycin) and 1% fetal bovine serum. The cells were sown in a 25 mL T-culture flask and kept in a humidified environment with 5% CO_2 at 37 °C. After the culture cells reach 70% confluence, the adipocyte cells undergo differentiation in Adipogenesis supplementation media called "DMEM" supplemented with 10% FBS, 100 IU of penicillin streptomycin, 0.15 IU/mL insulin, 500µM of dexamethasone, and 500µM isobutyl methyl xanthine to stimulate adipocyte maturation for 72 h. After differentiation, the primary adipocyte culture was expanded for various experiments. The medium was replaced, and the cell growth was monitored every three days. The underlying investigations were carried out via the expanded cells.

Inducing a High-Fat Diet (HFD) in Adipocytes

For the induction of a high-fat diet model using adipocyte cells to mimic the effects of a high-fat diet, the expanded cells are re-introduced into supplemented medium enriched with a greater concentration of fatty acids (Xiang et al., 2024). The incubation process is carried out for a further 7–14 days, with regular changes medium every 3 days. 10 µL of resuspension pellet cells were put onto a hemocytometer to calculate the number of cells that were required to be seeded for the tests. The cells in the four squares of the hemocytometer were counted averaged and multiplied by 10^4. Eventually, the HFD-AD were harvested conventionally using 0.025% Trypsin EDTA and divided into two parts. Each part is planted in 96 well plates at a density of 1×10^5 cells/well. The plates contained DMEM, supplemented with 10% FBS and 1% penicillin G sodium (10.000 UI), streptomycin (10 mg), and amphotericin B (25 µg) PSA, and incubated at 37 °C with 5% CO_2 for 48 hours. Culture medium was removed and replaced by new media after washing the cells three times with 10% PBS to remove any blood and induced as described previously (Yunusoglu et al., 2022). After 24 hours, the following experiments begin to work.

EC_{50} of EtOAc. Fr., and Aqueous Fr. on a High Fat Diet Adipose Tissue (HFD-AD)

EC_{50} of EtOAc. Fr. and aqueous Fr. was measured in high-fat diet adipocytes by EtOAc. Fr. and aqueous Fr. was measured by the Vybrant® MTT (3- 4,5-dimethyl-2-thiazolyl-2,5-diphenyl-2H-tetrazolium bromide) cell proliferation assay kit, cat no. M6494 (Thermo Fisher, Germany), with minor modifications provided by (Liu et al., 1997; Yunusoglu et al., 2022). Briefly, 1 mg/mL of each EtOAc. Fr. and aqueous Fr. stock solution was diluted with 1% DMEM (1 mL DMEM and 99 mL PBS) to create extracts at concentrations in the range of 0.001–100 µg/mL. After that, HFD-AD was exposed to EtOAc Fr., aqueous Fr., and MSM were tested at concentrations of 0, 0.01, 1.0, 10, and 100 µg/mL for 48 hours. The medium was removed and 12 µL of MTT solution (1 mg/mL) (Invitrogen, Thermo Scientific, Germany) was added to each well, and the plates were incubated at 37°C and 5% CO_2 for four hours. Finally, the MTT solution was removed, and 100 µL of sodium dodecyl sulfate with hydrochloric acid (SDS-HCL) was added to the wells. Cell viability was determined by measuring the optical density at 570 nm on a spectrophotometer (ELx 800; Bio-Tek Instruments Inc., Winooski, VT, USA), and the percentage of viability was determined, which represents the proliferative effect of the extract at the tested dilutions. The XY curve was plotted to illustrate the relationship between the log dose of the agonist and the normalized response. The best fit point was determined by linear regression analysis for the calculation of the half maximal effective concentration (EC_{50}). The relationship between the log dosage of the agonist and the normalized response was represented by the plotting of the XY curve. To compute the half maximum effective concentration (EC_{50}), linear regression analysis was used to identify the best fit point. The program Graph Pad Prism 9 was used to compute the EC_{50}.

EtOAc Fr., Aqueous Fr. and MSM Induction on HFD-AD

The study evaluates the ketogenic effect of EtOAc. Fr. and aqueous Fr. of the plant against control group on HFD adipocytes. Cultured cells of HFD-AD were harvested, washed, and planted in 96 well plates at a density of 1×10^5 cells/well as previously. The cells were treated with the values of EC_{50} of each EtOAc, aqueous and drug fractions individually and incubated in cell culture for 48 hours. Methylsulfonyl

methane (MSM) "Ketogenic which serves as the positive control. Negative control group was the only differentiation medium applied to the cells. Subsequently, several assays were employed to evaluate the impact of each extract on lipid metabolism, including measurement of lipid profile, assessment of oxidative and antioxidant effects, and detection of lipid accumulation by oil-red staining. All samples are run in triplicate.

Assessment of Lipid Accumulation in Adipocytes' Harvested Cells

A variety of measures were employed to evaluate the growth of an obesity-like phenotype. These include assessing the shape of the cell by enhancing the development of lipid droplets and using Oil Red O staining to show the accumulation of lipids.

Oil red O (ORO) Stain for Adipogenesis: Lipids accumulate in the adipocyte cell as a single lipid droplet during the development procedure. This suggests that white pre-adipocytes grown into adult white adipocytes (Konige et al., 2014). To assess the amount of lipid accumulation in adipocytes treated cells by EC_{50} values of EtOAc Fr., aqueous Fr. and MSM during the period of differentiation process (4-13 days), stained by ORO from Sigma-Aldrich (O0625) (Kraus et al., 2016). The differentiated cells were carefully washed with PBS after the culture media was aspirated to get rid of anything that remained. After that, the adipocytes were fixed by incubating them for half an hour at room temperature in 3.7% formaldehyde, cleaned with tap water three times and stained with a 3 mg/mL ORO solution in isopropanol for 15 minutes to see the lipid droplets. To get rid of extra ORO, the cells were cleaned three times using distilled water. Using an inverted microscope and labomed camera software (USA) to observe the mature cells which were stained with ORO. On other hand, Atlas 16MP Cmos USB Camera software, which is an image analysis program was used to examined photos.

Quantification the Lipid Content: The ORO dye was dissolved in DMSO and then added to a 96-well plate at volume 100 µL per well. The absorbance of each well was measured using a microplate reader at a wavelength of 510 nm on a spectrophotometer (ELx 800; Bio-Tek Instruments Inc., Winooski, VT, USA).

Measurement of Lipid Profiles

After removing the differentiation medium from the plate-based cells, it was washed with PBS three times, harvested, and homogenized with saline solution. The cells were collected for measurement of the lipid profile as well as the antioxidant and oxidative effects inside the cells, according to the manufacture of kits in triplicate.

Triglyceride Level: Triglycerides are fat-soluble molecules that are either stored in the liver or fat cells and give the body energy. High TG contributes to metabolic syndrome and obesity, which in turn lead to atherosclerosis (Ginsberg et al., 2021). TG content was determined using the End Point Colorimetric Triglycerides kit (cat. no. SU035; Reactivos GPL, Barcelona, Spain), which was based on the formation of a red quinone.

Cholesterol Level: Several metabolic functions, such as the production of certain hormones and cell development, depend on cholesterol. High levels of cholesterol can increase risk of heart disease (Rahmati et al., 2019). The end point colorimetric cholesterol kit (cat no. SU013; Reactivos GPL, Barcelona, Spain) measures the total quantity of cholesterol contained in the sample and finds a direct correlation with the intensity of the quinoneimine color

HDL-C: HDL collects and transports excess cholesterol from the blood stream to the liver, where it is processed and eliminated from body, and elevated HDL-C (good cholesterol) can lower your risk of heart disease and stroke (Sabatine et al., 2017). Using phosphotungstate to precipitate LDL and VLDL lipoproteins from serum or plasma in the presence of magnesium ions, the clear supernatant containing HDL is removed using centrifugation. Measuring HDL cholesterol using the End Point Colorimetric HDL-Cholesterol Kit (cat. no.: SU0141; Reactivos GPL, Barcelona, Spain).

LDL-C: The majority of the cholesterol in body is composed of LDL-C, frequently referred to as "bad" cholesterol. LDL-C at a high level increases the risk of heart disease (Lloyd-Jones et al., 2022). The LDL-C was calculated using the following equation: LDL-C = (Total Cholesterol – HDL-C) – TG/5.

Measurement of Oxidative Markers

MDA Level: An increase in the level of MDA represents an oxidative decomposition product of polyunsaturated fatty acids in the cells, a marker of lipid peroxidation and antioxidant status (Cordiano et al., 2023; Gaweł et al., 2004). The MDA was determined in serum by the Draper and Hadley method (1990) using the MDA colorimetric assay kit, catalog No: E-BC-K025-S, Elabscience Biotechnology,

USA. Utilizing the molar extinction coefficient of MSM (1.56 × 105 mol/L/cm), the quantity of the reactive chemical thiobarbituric acid was determined using the formula: A=ΣCL, the variables are absorbance (A), molar coefficient (Σ), concentration (C), and route length (L). The outcomes were given as µMol/L of sample.

NO Level: Superoxide or oxygen radicals react with nitric oxide to produce endogenous reactive nitrogen species which have been implicated in the pathogenesis of many diseases. cardiovascular dysfunction (Pacher et al., 2007). The amount of nitrite in the culture medium was measured as an indicator of NO production by the Colorimetric Assay Kit (catalog no. E-BC-K035-M, Elabscience Biotechnology, USA). The absorbance was measured at 550 nm on a microplate reader. The nitrite concentration was calculated using the sodium nitrite standard curve.

CAT Assay: The body's catalase enzyme facilitates the breakdown of hydrogen peroxide into water and oxygen to protect tissues from damage by peroxide, which is constantly created by a variety of metabolic processes (Nandi et al., 2019). Using the colorimetric kit, cat no: EBC-K031-S, Elabscience Biotechnology, USA. Samples were diluted by PBS (0.01 M, pH 7.4). In the range of 100–200 U/mL, the reaction that catalase decomposes H_2O_2 can be quickly stopped by ammonium molybdate. The residual H_2O_2 reacts with ammonium molybdate to generate a yellowish complex. CAT activity can be calculated by producing the yellowish complex at 405 nm. CAT activity can be calculated by producing the yellowish complex at 405 nm.

TAC Assay: By using the phosphomolybdenum technique, the total antioxidant capacity (T-AOC) of the EtOAc. Fr. and aqueous Fr. of the plant was evaluated by the Colorimetric Assay kit (cat. no. E-BC-K136-M, Elabscience Biotechnology, USA), with less modification according to the protocol described by Prieto et al. (1999). The absorbance was measured at 695 nm against a blank. Total antioxidant capacity (TAC) was expressed as tannic acid equivalent (TAE).

Statistical Methods & Analysis for Data

The gathered data had been revised, coded, tabulated, and placed on a PC using Graph Pad Prism Software (San Diego, US). The data are displayed as means, standard deviation (± SD), and range for parametric numerical data. After determining the statistical significance of the difference between more than two study group means using the Analysis of Variances (ANOVA) test, the Post-Hoc test was utilized to determine whether the three group means were equal. The P-values ≤0.05 and <0.01 are significant and highly significant, respectively.

RESULTS AND DISCUSSION

Lipase Inhibitory Assay *In vitro*

Lipase inhibitory assays are a common method for determining the potential of a natural product's anti-obesity drug (Abdel-Sattar et al., 2014). Pancreatic lipase inhibitory activity was evaluated for *E. r.* subsp. *schimperi* extract (crude ethanol, 70%). The inhibitory activity due to monitoring the transformation of *p*-nitrophenyl butyrate (pNPB) to *p*-nitrophenol by the crud extract *E. r* subsp. *schimperi* at different concentrations (0.25, 0.5, 1, 2,.., 500 µg/ml) had a moderate inhibitory effect with an IC_{50} 86.91± 4.3 µg/ml compared with the standard (Orlistat) followed by five fractions of the plant. The highest inhibition of lipase enzyme was for aqueous Fr. and EtOAc Fr. at IC_{50} of 18.15 ± 1.24 and 27.51 ± 2.94 µg/ml, respectively, followed by BtOH Fr., and $CHCl_3$ Fr., with IC_{50} of 55.64 ± 2.68 and 78.59 ± 40 µg/ml, respectively. Table1. The inhibitory effect of orlistat is still relatively higher than that of EtOAc Fr. and aqueous Fr. of the plant. Therefore, the effects of aqueous and ethyl acetate fractions were used to determine their ketogenic effect on HFD adipocyte cells at *ex vivo*.

EC_{50} of EtOAc. Fr., Aqueous Fr., and MSM in HFD-AD

The EC_{50} values in high-fat diet-induced adipose tissue (HFD-AD) cells treated with different concentrations of EtOAc. Fr., aqueous Fr., and MSM ranging from 0.001 to 100 µg/ml for 48 hours were evaluated. The EC_{50} values of EtOAc. Fr. and aqueous Fr. were 0.147±0.003 and 0.249±0.025 µg/ml, respectively (Figure 1). However, the EC_{50} of MSM is 0.093±0.02 µg/ml. EC_{50} of the EtOAc, aqueous and MSM fractions represented as doses to treatment obesity caused by a high-fat diet adipose tissue cell.

The ketogenic effect of EtOAc. Fr. and aqueous Fr. on HFD-AD cells

The ketogenic effect was evaluated for EtOAc. Fr. and aqueous Fr. on HFD-AD compared with untreated cells, and the lipid profiles (C, TG, HDL-C, and LDL-C), MDA, NO, CAT, and TAC were evaluated in the cells. All samples are run in triplicate.

Cell Morphology Using ORO and Lipid Content

The morphological investigation of HFD-AD cells treated with EtOAc. Fr. and aqueous compared by untreated cells by an inverted microscope with a 200x magnification shows Oil Red O staining of HFD adipocytes cells after treatment by EtOAc Fr., aqueous Fr. and MSM at doses of 0.147±0.003, 0.249±0.025 and 0.093±0.02 µg/ml for 48 hours, respectively. As a result, MSM minimized lipid droplets (size and numbers) followed by aqueous Fr. and EtOAc. Fr., respectively, compared to untreated cells Figure 2. EtOAc. Fr. and aqueous Fr. significantly reduce lipid content compared to untreated cells ($p<0.0001$); however, the aqueous Fr. exhibits a marked reduction in lipid content compared to EtOAc. Fr. ($p<0.0001$). Thus, the aqueous Fr. shows a significant decrease in lipid content (Figure 3).

Lipid Profile

Triglyceride Level: Figure 4a, demonstrated that EtOAc. Fr., aqueous Fr., and MSM significantly reduced triglycerides compared to HFD adipocytes ($p < 0.0001$). The aqueous Fr. performed better than EtOAc Fr. at mild significant difference ($p= 0.0026$). No significant difference was detected between the effects of aqueous Fr. and MSM on the triglyceride level $p=0.0539$. While the significant difference between MSM and EtOAc Fr. on the triglyceride level ($p=0.0001$).

Cholesterol level: Both fractions exhibit a significant effect on cholesterol levels compared to untreated cells. The treatment with aqueous Fr. caused a slight decrease in the level of cholesterol, whereas aqueous Fr. maintained a cholesterol level closer to MSM with a non-significant difference ($p = 0.2800$). The ANOVA analysis shows a non-significant difference in the cholesterol levels between all the groups ($p > 0.05$), except that there is a significant difference between the aqueous Fr. and EtOAc. Fr. groups ($p = 0.0163$) Figure 4b.

High-Density lipoprotein Cholesterol (HDL-C): The effects of EtOAc Fr., aqueous Fr. induced on HFD adipocytes significantly increase HDL-cholesterol levels compared to untreated cells ($p<0.05$). But the effect of aqueous Fr. is non-significant compared to MSM ($p = 0.8773$) and EtOAc. Fr. in comparison to MSM ($p = 0.4432$). Thus, the increase in HDL-C is particularly noticeable in aqueous Fr. (Figure 4c).

Low-Density lipoprotein Cholesterol (LDL-C): EtOAc Fr. and aqueous Fr. significantly reduce LDL-C levels compared to untreated cells. In contrast, no significant difference in LDL-C levels was associated with aqueous Fr. and MSM ($p > 0.05$). There was a significant difference between EtOAc. Fr. and MSM ($p = 0.0046$), as confirmed by the ANOVA analysis (Figure 4d).

Table1. Inhibition of lipase enzyme by the crude extract of plant and its fractions against the standard drug *in vitro.*

Fraction/ Drug	IC_{50} µg/ml
Crude extract	86.91 ± 4.31
Hex.Fr.	247.22 ±7.89
$CHCl_3$ Fr.	78.59 ± 4.31
EtOAc Fr.	27.51 ± 2.94
BtOH Fr.	55.64 ± 2.68
Aqueous Fr.	18.15 ±1.24
Orlistat	5.27 ± 0.62

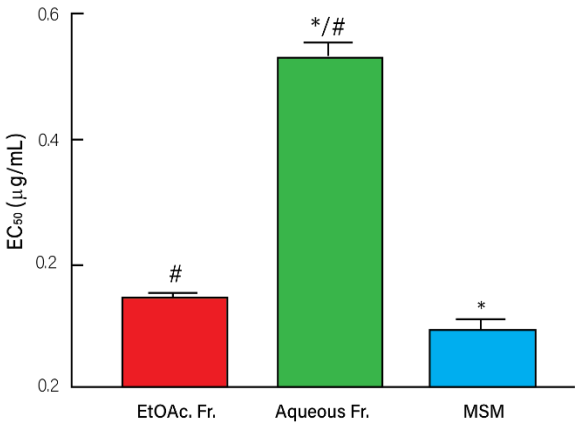

Figure 1. EC_{50} of EtOH Fr, aqueous Fr. and MSM in HFD-AD. Data are presented as mean and standard deviation. *: significant difference compared to EtOH Fr., #: significant difference compared to MSM.

Oxidative Markers

Malondialdehyde level: The level of MDA was significantly decreased in the HFD-AD cells treated by aqueous Fr. compared to untreated cells; however, EtOAc. Fr. did not. The impact of aqueous Fr. and MSM on the MDA level did not differ significantly ($p > 0.05$) Figure 5a. This reduction in MDA may indicate that the aqueous had an improved antioxidant capacity.

Nitric oxide level: The effect of MSM, EtOAc. Fr., and aqueous Fr. on HFD adipocytes significantly reduced nitric oxide levels compared to untreated cells ($p<0.05$). The non-significant of the aqueous Fr. vs. MSM $p>0.05$. This demonstrates the substantial effect of the aqueous Fr. on nitric oxide levels Figure 5b.

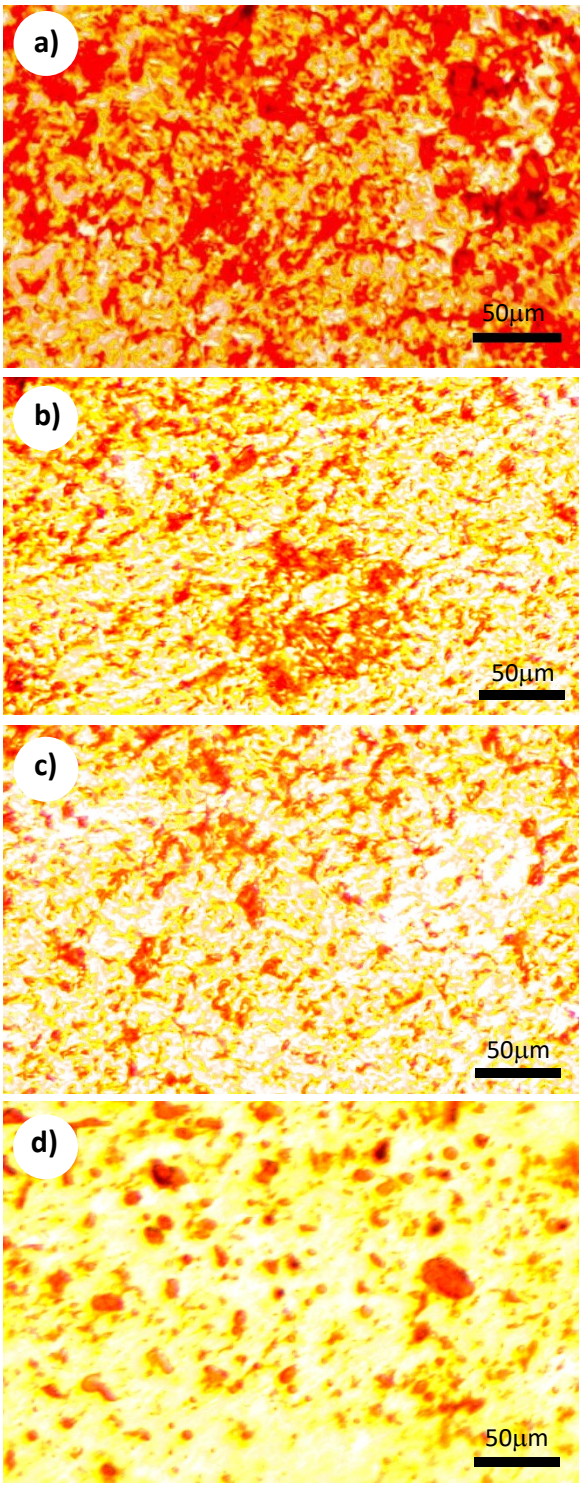

Figure 2. (a) untreated HFD adipocytes, (b) cells incubated with EtOAc. Fr. (c) cells incubated with aqueous Fr. (d) cells incubated with MSM. Photomicrographs show Oil Red O staining of cells 48 hours after incubation Magnification, x200. The upper images show the cells morphology captured with using an inverted microscope LABOMED. camera software, USA), and the images analyzed by the image analysis software (Atlas 16MP Cmos USB Camera software).

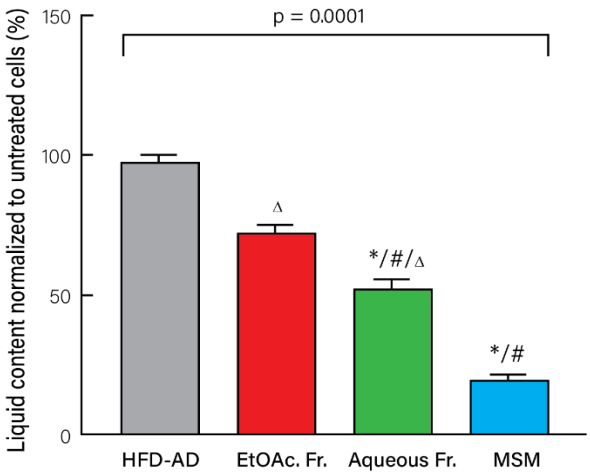

Figure 3. The lipid content in each group after being normalized to the untreated cells. *: statistical significance compared to the untreated cells (NC), #: statistical significance compared to the EtOAc. Fr. treated cells, Δ: statistical significance compared to the MSM (PC).

Antioxidant Effect in HFD Adipocytes

Catalase level: In contrast with HFD-AD cells, aqueous and MSM fractions dramatically increase catalase activity Figure 5c. Compared to MSM, the aqueous Fr. significantly increased the level of CAT enzyme ($p = 0.0036$). In reverse, the influence of EtOAc. Fr. compared to MSM showed a significant difference at $p = 0.0006$.

Total Antioxidant Capacity: A significant increase in TAC was associated with the incubation of differentiated cells with aqueous Fr. and EtOAc. Fr. compared with HFD-AD in Figure 5d. There is a marked increase in the level of TCA in HDF AD treated by aqueous Fr. compared to MSM, with a significant difference of $P = 0.0062$. While EtOAc. Fr. versus MSM had $p<0.0001$.

According to the previously mentioned data, the hydroethanolic extract of *E. r*. ssp. *schimperi* aerial parts possessed an inhibition of the lipase enzymes *in vitro* with an IC_{50} 86.91 ± 4.3 µg/mL, and by using bioassay-guided fractionation for crude extract to give Hex. Fr., $CHCl_3$ Fr., EtOAc. Fr., BtOH Fr., and aqueous Fr., the fractions were screened also for the inhibition of the lipase enzymes *in vitro*. The findings indicated that the aqueous Fr., of the plant showed the greatest inhibition of lipase enzymes at IC_{50} 18.15 ± 1.24 µg/ml, followed by the EtOAc. Fr. at IC_{50} 27.51 ± 2.94 µg/ml. This result was confirmed by Jaradat et al. (2017). Meanwhile, EtOAc. Fr., aqueous Fr. and

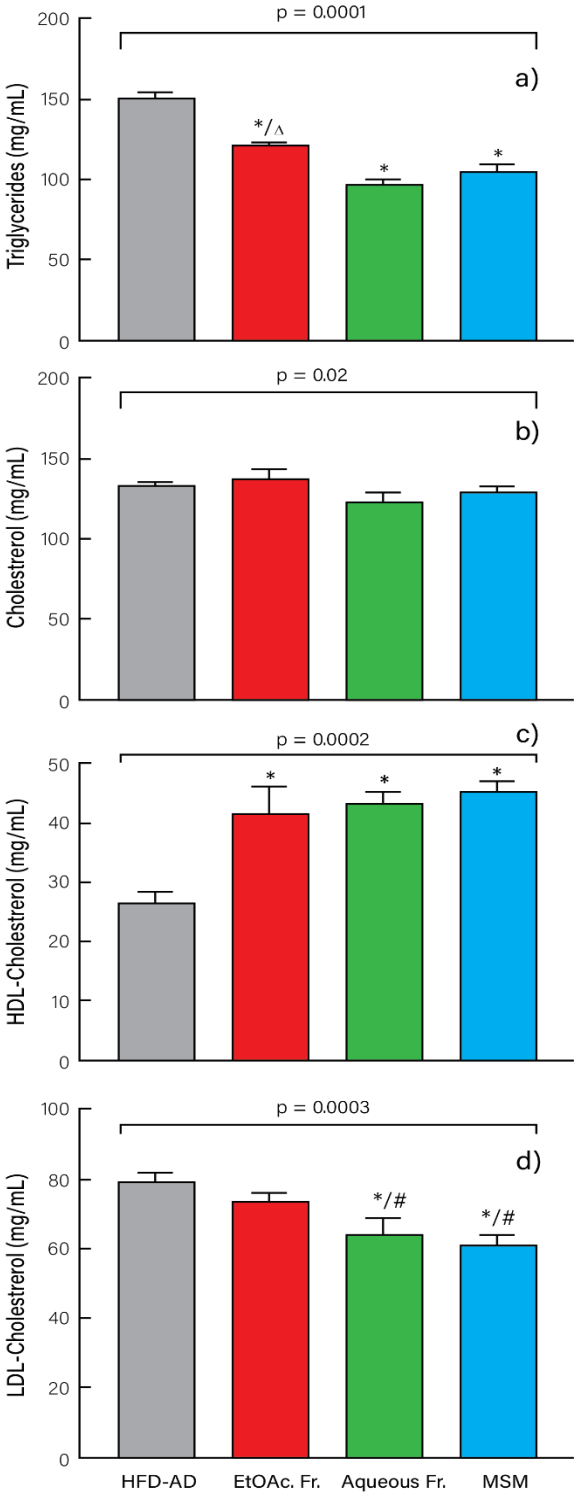

Figure 4. Ketogenic effect of EtOHAc.Fr. and Aqueous Fr. in HFD-adipocytes cells. (a) Triglycerides in culture media, (b) Total Cholesterol level, and (c) HDL-cholesterol level, (d) LDL-cholesterol level. Data are presented as mean and standard deviation. *: statistical significance compared to the untreated cells (NC), #: statistical significance compared to the EtOAc. Fr. eated cells, Δ: statistical significance compared to the MSM (Positive control, PC).

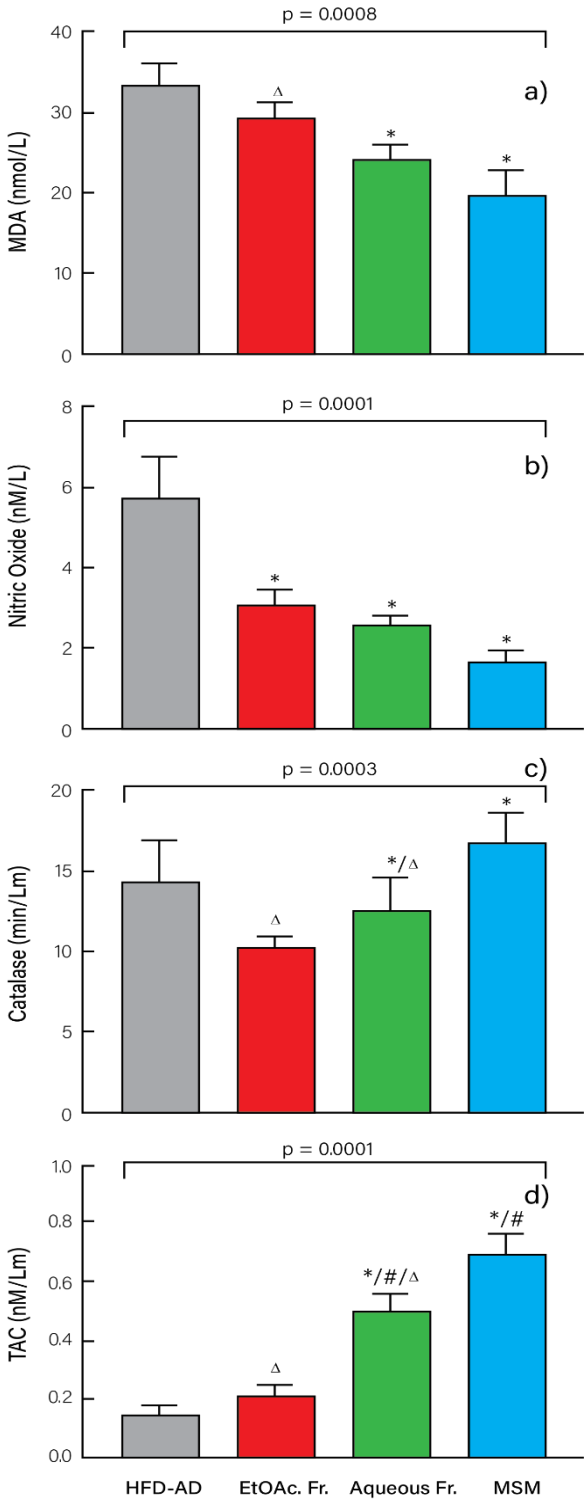

Figure 5. Antioxidative effect of EtOAc. Fr. and aqueous Fr. in HFD-adipocyte cells. (a) malonaldehyde level in culture media; (b) nitric oxide level; (c) catalase activity; and (d) TAC. Data are presented as mean and standard deviation. *: statistical significance compared to the untreated cells (NC), #: statistical significance compared to the EtOAc. Fr. treated cells, **Δ**: statistical significance compared to the MSM.

MSM on HFD-AD cells at doses of 0.147±0.003, 0.249±0.025 and 0.093±0.02 µg/ml, respectively, *ex vivo* established that, the aqueous Fr. significantly decreased the levels of triglycerides, cholesterol, LDL-C, lipid content and lipid droplet (size and numbers). It also improved HDL-C in HFD adipocytes compared to EtOAc. fraction. Moreover, the aqueous Fr. reduced the oxidative marker (MDA and NO) levels and increased the antioxidant markers (CAT and TAC). As a result, the aqueous Fr. may reduce fat by lowering adipogenesis, blocking adipocyte differentiation, and improving lipid metabolism. Hence, the aqueous Fr. may have an antiobesity impact by treating HFD-induced obesity, boosting energy consumption, alleviating metabolic disorders by improving lipid profiles, reducing oxidative stress, and enhancing antioxidant defense. The impact of the aqueous Fr. on HFD-AD could be attributed to the presence of antiobesity phenolic compounds from various classes, including flavonoids, phenolic acids, coumarin derivatives, and pentacyclic triterpenes, as analyzed by LC-ESI-MS/MS. These compounds aid in obesity management by enhancing calorie consumption, reducing adipogenesis, preventing adipocyte differentiation, and modulating lipid metabolism, as mentioned in earlier research (Yen et al., 2020). The bioavailability, metabolism, and biological activity of phenolic compounds depend upon the configuration, total number of hydroxyl groups, and substitution of functional groups (Kumar and Pandey, 2013). Flavonoid O-glycosides hydrolyze readily to produce their aglycone, which may be absorbed by cells quickly (Xie et al., 2022). The aqueous fraction was proven to include several well-known antiobesity agents including flavonoids that were most found in the fraction: flavanol, flavone, and their O-glycosides. The predominant flavonoid in this fraction is myricetin-O-rhamnoside, which in previous research (Kim et al., 2019) showed that it increases energy exhaustion and decreases hepatic triglyceride accumulation, fatty acid synthase in the liver, adipocyte size, adipose tissue mass, and dyslipidemia. Also, myricetin had a modified antiobesity effect by preventing diet-induced obesity, reducing oxidative stress, hypercholesterolemia, and hypertriglyceridemia. According to Su et al. (2016), quercetin and luteolin convert white adipocytes to brown, enhance energy consumption, and improve the metabolism of fat and glucose to prevent weight gain and metabolic diseases (Zhang et al., 2019). Additionally, on a high-fat diet, quercetin prevents obesity and metabolic disorders by improving antioxidant levels, adipogenesis, and adipose tissue inflammation (Dong et al., 2014). Furthermore, kaempferol enhanced antioxidant defense by reducing lipid peroxidation and suppressing lipid accumulation (Hossain et al., 2016). Gallic acid regulates adipocyte hypertrophy and suppresses inflammatory gene expression induced by the paracrine interaction between adipocytes and macrophages *in vitro* and *in vivo* (Tanaka et al., 2020). Ethyl gallate diminished the early stage of adipogenesis in 3T3-L1 cells by decreasing PPARγ and C/EBPα expression levels, which could induce adipogenesis (Ahn et al., 2022). *p*-Coumaric acid inhibited the development of preadipocytes and skeletal muscles by minimizing the primary transcription factors and their related diseases (Ilavenil et al., 2016). Also, Yang et al. (2024) found that esculin reduces the effects of obesity-induced insulin resistance by enhancing adipose tissue remodeling and stimulating the PI3K/IRS1/GLUT4/AKT pathway. Mohsen et al. (2019) stated that betulinic acid is an effective therapy for the prevention of obesity and may be able to modify cofactors to control PPAR gamma activation. Also, it prevents abdominal fat accumulation in mice fed a high-fat diet (Lin et al., 2009). Additional research showed that pancreatic lipase activity was inhibited by oleanolic acid (OA) (Oboh et al., 2021). Besides, OA suppressed the inflammatory response during adipocyte development, and nano-OA was effective in treating the metabolic dysfunction that a high-fat diet causes in rats (Feng et al., 2020). Finally, asiatic acid is a hepatic protective agent against liver damage caused by a high-fat diet (Yan et al., 2014), and arjunolic acid showed a high potency as an antioxidant (Ghosh and Sil, 2013).

LC- ESI-MS/MS for Aqueous Fr.

In this study, twenty-five compounds were tentatively identified in the aqueous Fr. of *E. r.* ssp. *schimperi* by LC-ESI-MS/MS in both positive and negative ionization modes. The identification of compounds in this fraction was based on mass fragmentation patterns and the standard data reported in the published literature and database. The compounds in Table 2 were positioned in accordance with RT, including phenolic acid, flavonoids, and pentacyclic triterpenes, and contained O-glycosides. In previous research, they were easily broken down by hydrolysis to give neutral fragments corresponding to the sugar units and aglycone (Xie et al., 2022; Kachlicki et al., 2016).

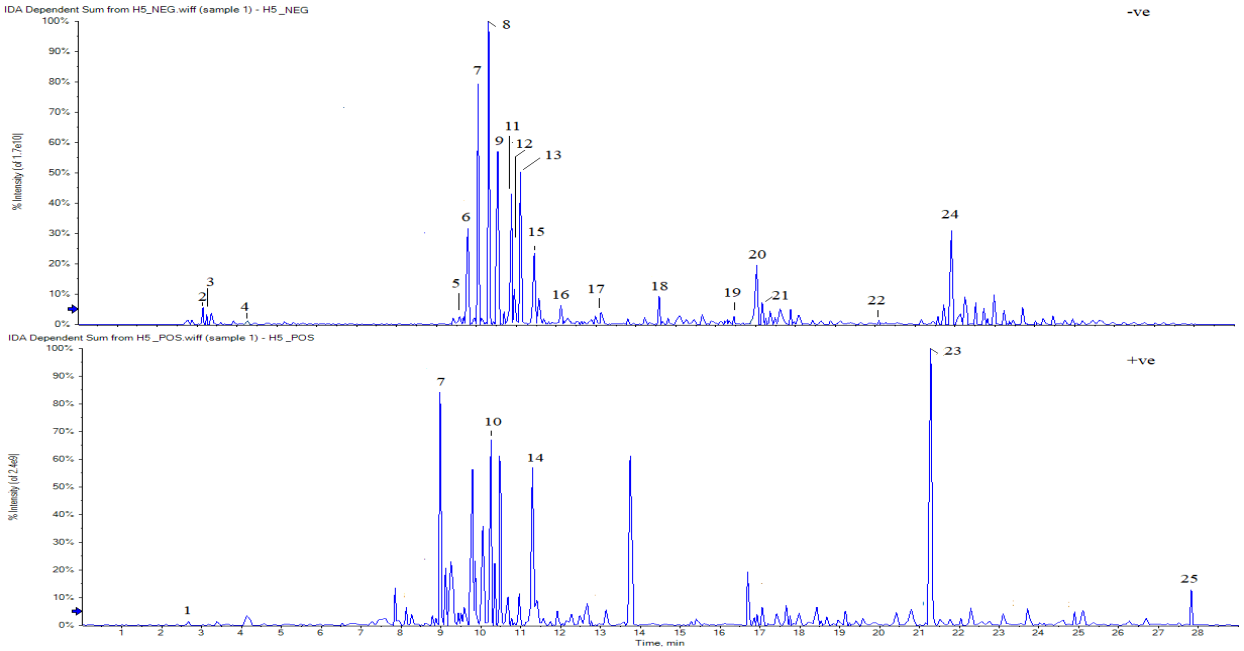

Figure 6. LC-ESI-MS –ve (a) and +ve (b) modes. of E.r subsp. schimperi aqueous fraction.

Table 2. The suggested compounds in the aqueous Fr. by LC ESI-MS/MS analysis in both negative and positive ionization modes.

NO	RT (min)	MWt.	-ve/ +ve	MS/MS fragments	Tentatively compound	Reference
1	2.668	$C_9H_8O_3$	+ 164.9	163, 146, 119	p-Coumaric acid	Razgonova et al., 2021.
2	3.147	$C_7H_6O_5$	- 169	124.97, 106.98	Gallic acid	Shi et al., 2022. Boritnaban et al., 2022.
3	3.210	$C_8H_8O_5$	- 183	168.15, 124 ,6, 109, 78.02	Methyl gallate	Singh et al., 2016.
4	4.278	$C_{13}H_{16}O_{10}$	- 331	169, 153, 125	O-galloylglucose	Singh et al., 2016.
5	9.681	$C_{15}H_{17}O_{11}$	- 371	209, 191.	caffeoyl glucaric acid isomers	Fernández-Poyatos et al., 2019.
6	9.823	$C_{21}H_{20}O_{13}$	- 479	333-331-317	myricetin-O-β-D- hexoside	Blajan et al., 2006.
7	9.014 10.076	$C_{21}H_{20}O_{12}$	+ 465 - 463	464.9, 319, 318, 273.09, 179.02, 174.7,152.09, 316,271, 179, 151	Myricetin-O-deoxyhexose	Rached et al., 2017. Nguyen et al., 2013.
8	10.308	$C_{21}H_{20}O_{12}$	- 463	316,271, 179, 151	Myricetin-O-deoxyhexose	Rached et al., 2017.
9	10.572	$C_{21}H_{20}O_{12}$	- 463	316,271, 179, 151	Myricetin-O-deoxyhexose	Rached et al., 2017.
10	10.352	$C_{15}H_{10}O_8$	+ 319	318.89, 272, 216, 164, 152, 137	Myricetin	Nguyen et al., 2013.
11	10.883	$C_{23}H_{24}O_{12}$	- 493	492.96, 316, 271, 151	myricetin-O-glucuronide	Barbosa et al., 2006.
12	10.943	$C_9H_{10}O_5$	- 197	168.97, 140.03, 124.99 78.01	Ethyl gallat	Singh et al., 2016.
13	11.136	$C_{21}H_{20}O_{11}$	- 447.4	446,9, 3013, 300, 271, 255., 179, 151.	Quercetin-O- rhamnoside	Pereira *et al.*,2017. Kerebba *et al.*, 2022.
14	11.413	$C_{15}H_{10}O_7$	+ 303	303, 302	Quercetin	Jang et al., 2018.
15	11.452	$C_{21}H_{19}O_{10}$	- 431	431, 285.0, 255, 227	Kaempferol O- rhamnoside	Li et al., 2016. Hassan et al., 2018.
16	12. 215	$C_{27}H_{30}O_{15}$	- 593	593, 447, 284.97, 256.9, 243, 241,199, 151, 132.9	Luteolin O –rutinoside	Brito et al., 2014.
17	13.196	$C_{15}H_{10}O_6$	- 285	284.96, 217.12, 199.12, 151.08, 133,09	Luteolin	Sliwka-Kaszynska et al., 2022; Brito et al.,2014.
18	14.586	$C_{30}H_{48}O_5$	- 487.2	469.40, 421.3, 409.31, 379, 277.2, 203.2, 221.2	2a, 3a, 24-trihydroxyurs-12-en-28-oic acid	Ceccacci et al., 2022. Xia et al., 2015.
19	16.462	$C_{15}H_{16}O_9$	- 339	337, 293, 194, 178, 177, 173, 149, 131	Esculin	Abd El Aziz et al., 2024
20	17.065	$C_{36}H_{56}O_9$	- 631	631.3, 455.1	Oleanolic acid-O-glucuruopyranosyl	Ngoc et al., 2022
21	17.202	$C_{30}H_{48}O_4$	- 471	453, 425, 380, 203, 177.	Hydroxy betulinic acid.	Okba et al., 2021.
22	20.91	$C_{40}H_{58}O_5$	- 617	617, 455.2, 407,391, 377, 363, 203	Oleanolic acid 3-O-α-glycoside	Ngoc et al., 2022.
23	21.331	$C_{30}H_{48}O_3$	+ 457	248, 203, 207, 189, 175.	betulinic acid	Abdel Ghani *et al.*, 2023.
24	21.946	$C_{30}H_{50}O_3$	- 455.5	407, 391, 377, 363, 203	Oleanolic acid	Chen *et al.*, 2011.
25	27.901	$C_{30}H_{49}O_2$	+ 441	382, 205, 189, 163, 107	(20S)-3-Oxolupan-30-al	Mutai *et al.*,2007.

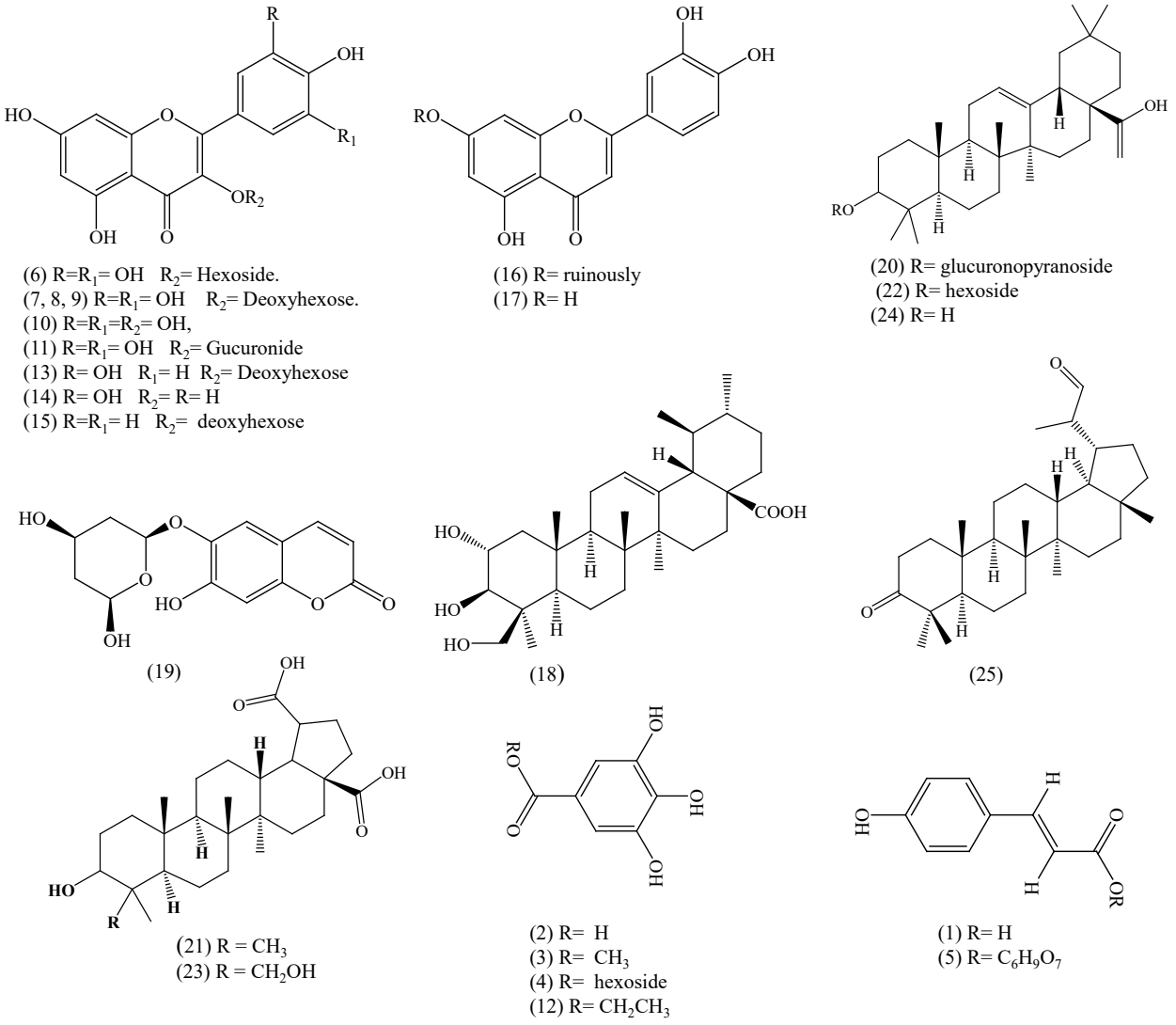

Figure 7. Basic structures of the 25 phytochemical compounds that have been tentatively identified from the aqueous fraction by LC ESI-MS/MS analysis : (1) p-coumaric acid, (2) gallic acid, (3) methyl gallate, (4) O-galloylglucose, (5) caffeoyl glucaric acid isomers, (6) myricetin-3-O-β-D-hexoside, (7, 8, 9) Myricetin O-deoxyhexose, (10) Myricetin, (11) myricetin -O-glucuronide, (12) ethyl gallat, (13) quercetin - O- rhamnoside, (14) quercetin, (15) Kaempferol -O rhamnoside, (16) Luteolin- O –rutinoside, (17) Luteolin (18) 2a, 3a, 24-trihydroxyurs-12-en-28-oic acid, (19) Esculin, (20) oleanolic acid-O-glucuruopyranosyl, (21) Hydroxy betulinic acid, (22) Oleanolic acid 3-O-α-glycoside, (23) betulinic acid, (24) Oleanolic acid, (25) (20S)-3-Oxolupan-30-al.

Some of the mass spectra of those phenolic compounds showed the aglycone ion as myricetin, quercetin, kaempferol, luteolin, and oleanolic acid as a result of the loss of sugar moieties like deoxyhexosyl (rhamnose), hexosyl (glucose or galactose), glucuronyl (glucuronic acid), and ruinously (-146, -162, -176, and -308 Da), respectively (Llorent-Martínez et al., 2015). The structures of the most relevant compounds are shown in Figures 6 and 7 and listed in Table 2.

Phenolic Acids. Peaks 2, 3, 4, and 12 represent phenolic acids. Gallic acid was discovered to be the [M-H]- ion peak 2 at m/z 169.01 (Shi et al., 2022; Boritnaban et al., 2022). The loss of CO2 (-44 Da) resulted in a base peak at m/z 124.97, while the combination of CO2 and H2O at -62 Da gave rise to a peak at m/z of 106.98. The peaks at m/z of 125 and 107 confirmed gallic acid. Peaks 3 and 12 were discovered at m/z 183.03 and 197.05, which matched the $[M-H]^-$ ions of methyl and ethyl gallate. Fragmentation showed peaks at 168.07 and 168.97, respectively, and further fragments at 124.6 $[M-H-CH_3-CO_2]^-$ and 124,99 $[M-H-C_2H_5-CO_2]^-$. These compounds have been verified according to Singh et al. (2016), peak 4, molecular ion at m/z 331, $[M-H]^-$ resulted in the elimination of hexose moiety (-162) to

yield gallic acid at m/z 169. Our result suggested that the peak was *O*-galloylglucose and it was confirmed by the literature as a type of tannin (Singh et al., 2016). Peak 5 suggested that the compound was postulated to be caffeoyl glucaric acids. The peak ion detected at m/z 371 $(M-H)^-$ lost a caffeoyl group (m/z -162) to give fragmentation patterns at m/z 209 and 191 in the negative mode, which indicated glucaric acid. The literature supported our findings (Fernández-Poyatos et al., 2019). Peaks (1) p-coumaric acid at m/z 165 $[M+H]^{+,}$ p-coumaric acid exhibited a base peak at m/z 119 (M-H-44) due to the loss of CO_2. Our findings were verified by previous research (Razgonova et al., 2021).

Coumarin Derivatives: Peak 19 suggested esculin at $[M-H]^-$ m/z 339.13. Esculin was identified with fragment ion m/z 177, which refers to the loss of m/z -162 hexoside moiety with fragmentation pattern (173, 149, and 131). Our result was supported by the library of LC-mass spectra of aquoeus Fr. and confirmed with [Abd El Aziz et al., 2024].

Flavonoid Compounds: They were the predominant compounds in the aqueous Fr., with a special focus on myricetin deoxyhexose, which was seen at peaks 7, 8, and 9 molecular ions showed at m/z 463 $(M-H)^-$ and fragmentation gave myricetin aglycon at m/z 318 due to the released deoxyhexose moiety (-146). The findings we obtained were supported by before studies (Rached et al., 2017). Additionally, it was in a positive manner at peak 7 m/z 465 $(M+H)^+$ (Nguyen et al., 2013). Also, peaks 6 and 11, at m/z 479 $(M-H)^-$ and m/z 493 $(M-H)^-$ were tentatively identified as myricetin-3-O-hexoside and myricetin-3-O glucuronide, respectively, where they lost the hexoside moiety (-162) and the glucuronic acid (-176). The findings we obtained were supported by earlier studies (Blajan et al., 2006; Barbosa et al., 2006). Myricetin aglycone is produced by all peaks 6, 8, 7, 9, and 11, fragmented at 317, 271, 151, 137 in the -ve mode and at 319, 273, 153 in the +ve mode. Additionally, Peak 10 probably showed that myricetin aglycone produced molecular ion $(M+H)^+$ at m/z 319 and that it exhibited distinctive fractionation at m/z 318, 151, and 137. These findings were corroborated by the results reported by Thuan et al. (2013). Furthermore, the peak 15 at m/z 431 $(M-H)^-$ kaempferol-3-O-deoxyhexose was estimated and gave a fragment at m/z 285.0 corresponding to kaempferol, which was identified as an aglycone by the characteristic fragments at m/z 255 and 227 (Li et al., 2016) due to the elimination of -146 deoxyhexose. Our findings aligned with the published data (Hassan et al., 2018). Moreover, compound (13) exhibited at m/z 447 $[M-H]^-$ with a fragment peak at 301 $(M-H-146)^-$, which was ascribed to the removal of the deoxyhexose moiety and gave fragments at m/z 301, 271, 285, 179, and 151, indicating quercetin (Pereira et al., 2017). As a result, the peak was possibly recognized as quercetin-3-O-rhamnosid, or quercetrin, our findings concur with (Kerebba et al., 2022). Besides, quercetin aglycone peak 14 detected at $(M+H)^+$ m/z 303, present in library data of LC MS/MS analysis of aqueous Fr. of the plant and fragmentation of it gave ion peak at m/z 302 similar to the literature data at (Jang et al., 2018). Added to that, flavone peak 16 showed $[M-H]^-$ ion at m/z 593 was probably identified as luteolin O- rutinoside loosed of m/z -146 deoxyhexose, which on further loss of 162 (hexoside moiety) to produced ion peak at m/z 285 which is luteolin with characteristic fragment patterns of 284.99, 267, 217, 151, and 133 in peak 17 in negative mode supported by literature data (Sliwka-Kaszynska et al., 2022; Brito et al., 2014).

Pentacyclic Triterpenes: Four pentacyclic olean-type triterpenes the structure of 2α, 3β, 23-trihydrolean-12-en-28-oic acid (arjunolic acid), a peak (18) is suggested at m/z 487.3 $(M-H)^-$. Our results correlated with other studies, which found fragmentation patterns of 469.40, 421.3, 409.31, 379 and 203 (Ceccacci et al., 2022; Xia et al., 2015). Abase peak of oleanane and ursane type m/z 203 (Lourenço et al., 2021). Peak (24) was identified as oleanolic acid showed a typical peak ion at m/z 455 and revealed fragmentation at m/z 407, 391, 377, 363, and 203, corresponding to fragments of deprotonated oleanolic acid aglycone, which was confirmed by (Chen et al., 2011). Besides that, Peak (20) showed molecular ions $[M-H]^-$ was exhibited at m/z 631. The peak's fragmentation revealed peak at m/z 455 (aglycone of oleanolic acid) that was produced due to the loss of glucuronic acid (-176). This compound is oleanolic acid-O-glucuruopyranosyl. The results that we obtained were validated by research (Ngoc et al., 2022). Also, peak (22) at m/z 617 $(M-H)^-$ loosed H_2O (-18), C2O (-44) and -120 (characteristic of hexose fragmentation) to give m/z 455 (oleanolic acid aglycone), This saponin could therefore be attributed to the oleanolic acid O-glucopyranoside Our outcomes are reinforced by prior research (Ngoc et al., 20).

Three pentacyclic lupane-type triterpenes. Peak (25) revealed a molecular ion at m/z 441.1 $[M + H]^+$ was suggested to be 20S-3-Oxolupan-30-al. The compound showed a fragment peak at m/z 382 [(M +

H) – 59]$^+$, revealing the loss of aldehyde and ethyl groups from m/z 441 in addition, m/z 205, 189, 163, and 107. Our result is described by (Mutai et al., 2007). According to the peak (21) mass spectrum, the molecular ion at m/z 471 [M-H]$^-$. This ion fragmented at m/z 453 (M-H-CO) and m/z 425 (M-H- 2CO). Peak patterns at 380, 203, and 177 are also present. This implied the presence of hydroxybetulinic acid. The outcomes acquired by previous research (Okba et al., 2021). A molecular ion at m/z 457 [M+H]$^+$ was observed at peak (23), which was tentatively identified as betulinic acid. Other fragments were betulinic acid-specific MS2 fragment ions at m/z 248 [C16H24O2]$^+$, 203 [248-COOH]$^+$, 189 [207-H2O]$^+$, and 175 (Abdel Ghani et al., 2023).

CONCLUSION

The results of this investigation demonstrated that the aqueous fraction of *E. racemosa* subsp. *schimperi* was a potent inhibitor of lipase enzymes and that it decreased adipogenesis in HFD-AD cells. This was confirmed by a significant reduction in the levels of TG, C, LDL-C, lipid content, and lipid droplets (number and size) and increased HDL-C. Furthermore, the aqueous fraction showed an increase in CAT and TAC and a decrease in MDA and NO. These results were linked to many compounds from various classes that were detected by LC-MS/MS in the aqueous fraction. Thus, the aqueous fraction may have an antiobesity effect, with enhancing lipid profile, lowering oxidative stress, and strengthening antioxidant defence. Considering the published data, most of these results showed statistical significance, which supports the validity of our findings. Further research and clinical trials may be needed to fully understand the therapeutic effects of the compounds isolated from the plant against obesity.

ACKNOWLEDGEMENTS

The author offers gratitude and thanks to the Desert Research Center, Mataria, Egypt, as the herbarium for verifying the authenticity of the plant sample, which was gracefully done by Associate Professor Mahmoud Ali, and to the National Research Center, for LC-ESI-MS analysis, and to Faculty of Medicine, Ain Shams University for conducting the cellular experiments, with generous assistance from Prof. Dr. Nashwa El-Khazragy.

REFERENCES

Abd El Aziz, M.N., Hifnawy, M.S., Lotfy, R.A., Younis I.Y. (2024) LC/MS/MS and GC/MS/MS metabolic profling of *Leontodon hispidulus*, in vitro and *in silico* anticancer activity evaluation targeting hexokinase 2 enzyme. *Scientific Reports*, 14: 6872- 98. https://doi.org/10.1038/s41598-024-57288-4.

Abdel Ghani, A.E., Al-Saleem, M.S.M., Abdel-Mageed, W.M., Abou-Zeid, E.M., Mahmoud. M.Y., Abdallah R.H. (2023) UPLC-ESI-MS/MS profiling and cytotoxic, antioxidant, anti-inflammatory, antidiabetic, and antiobesity activities of the non-polar fractions of *Salvia hispanica* L. aerial parts. *Plants (Basel)*, 12(5): 1062-1079. https:// doi: 10.3390/plants12051062.

Abdel Raoof, G.F. (2022) Anti-obesity potential of natural products. *Egyptian Journal of Chemistry*, 65(10): 329 – 358. https://doi. 10.21608/EJCHEM.2022.118996.5354.

Abdel-Sattar, E., El Zalaban, i S. M., Salama, M.M. (2014) Herbal and microbial products for the management of obesity. *Anti-Obesity Drug Discovery and Development*, 2 (3): 130-210. https:// doi: 10.2174/9781608-059140114020005

Ahn, D., Kim, J., Nam, G., Zhao, X., Kwon, J., Hwang, J.Y., Kim J.K., Yoon, S.Y., Chung, S.J. (2022) Ethyl gallate dual-targeting ptpn6 and PPARγ shows anti-diabetic and anti-obese effects. *International Journal of Molecular Sciences*, 23(9):5020. https://doi.10.3390/ijms23095020 License CC BY 4.0.

Alias, N., Leow, T.C., Ali, M.S.M., Tajudin, A.A., Salleh, A.B., Abd Rahman, R.N.Z.R. (2017) Anti-obesity potential of selected tropical plants via pancreatic lipase inhibition. *Advances in Obesity, Weight Management & Control*, 6(4):122–131. https://doi.org/ doi.:10.15406/aowmc.2017.06.00163.

Al-Rawi, N.H. (2019) Oxidative stress, antioxidant status and lipid profile in the saliva of type 2 diabetics. *Diabetes & Vascular Disease Research,* 8(1) 22–28. https://doi.org/10.1177/1479164110390243.

Asres, K., Gibbons, S., Bucar, F. (2006) Radical scavenging compounds from Ethiopian medicinal plants. *Ethiopian Pharmaceutical Journal*, 24(1):24-28. https://doi.org/ doi. 0.4314/epj. v24i1.35095.

Barbosa, W.L.R., Peres, A., Gallori, S., Vincieri, F.F. (2006) Determination of myricetin derivatives in *Chrysobalanus icaco* L. (Chrysobalanaceae). *Revista Brasileira de Farmacognosia Brazilian Journal of Pharmacognosy*. 16(3): 333-337. https://doi.org/10.1590/S0102-695X2006000300009.

Batia, K. Baetia, P.B., Gaobotsea, G., Kwape, T.E. (2024) Leaf extracts of *Euclea natalensis* A.D.C ameliorate biochemical abnormalities in high-fat-low streptozotocin-induced diabetic rats through modulation of the AMPK-GLUT4 pathway. *Egyptian Journal of Basic and Applied Sciences*, 11(1): 232–252. https://doi.org/10.1080/2314808X.-2024.2326748©.

Bhardwaj, M., Yadav, P., Vashishth, D., Kavita, S., Kumar, A., Chahal, J., Dalal, S., Kataria, S.K. (2021) A review on obesity management through natural compounds and a green nanomedicine-based approach. *Molecules*, 26 (11): 3278- 3306. https://doi:10.3390/molecules-26113278

Blajan, K. Abliz, Z., Shang, X.Y., He, J.M., Zhang, R.P. Shi, J.G. (2006) Structural characterization of flavonol 3,7-di-O-glycosides and determination of the glycosylation position by using negative ion electrospray ionization tandem mass spectrometry. *Journal of Mass Spectrom*. 41:352–360. https://doi.org/10.1002-/jms.995.

Boritnaban, D.A., Karomah, A.H., Septaningsih, D.A., Majiidu, M., Dwiyanti, F.G., Siregar, I.Z., Rafi, M. (2022) Metabolite profiling of ebony (*Diospyros celebica* Bakh) leaves and wood extracts using LC-MS/MS. *Indonesian Journal of Chemistry*, 22 (2): 352 – 360. https://doi.org/10.22146/ijc.68529

Brito, A., Ramirez, J.E., Areche, C., Sepúlveda, B., Simirgiotis, M.J. (2014) HPLC-UV-MS profiles of phenolic compounds and antioxidant activity of fruits from three citrus species consumed in Northern Chile. *Molecules*, 19(11):17400-17421. https://doi.org/10.3390/molecules-191117400.

Ceccacci, S., Lucia, A. D., Tortora, A., Colantuono, A., Carotenuto, G., Tito, A., Monti, M.C. (2022*) Jasminum sambac cell* extract as antioxidant booster against skin aging. *Antioxidants (Basel)*, 11(12):2409- 2424. https://doi.org/doi: 10.3390/antiox11122409.

Chen, Q., Zhang, Y., Zhang, W., Chen, Z. (2011) Identification and quantification of oleanolic acid and ursolic acid in Chinese herbs by liquid chromatography–ion trap mass spectrometry. *Biomedical Chromatography*, 25 (12): 1381–1388. https://doi.org/doi: 10.1002/bmc.1614. Epub

Čolak, E., Pap, D. (2022) The role of oxidative stress in the development of obesity and obesity-related metabolic disorders. *journal of medical biochemistry*, 40(1): 1-9. doi: 10.5937/jomb0-24652.

Cordiano, R. Gioacchino, M.D., Gioacchino, M.D., Mangifesta, R., Panzera, C., Gangemi, S., Minciullo, P.L. (2023) Malondialdehyde as a potential oxidative stress marker for allergy-oriented diseases: an update. *Molecules*, 28(16): 5979. https://doi.org/10.3390/molecules28165979.

Croft, A.J., Kelly, C., Chen, D., Haw, T.J., Sverdlov, A.L., Ngo, D.T.M. (2023) Overexpression of mitochondrial catalase within adipose tissue does not confer systemic metabolic protection against diet-induced Obesity. *Antioxidants*, 12(5), 1137. https://doi.org/10.3390/antiox12051137

Dong, J., Zhang, X., Zhang, L., Bian, H.X., Xu, N., Bao, B., Liu, J. (2014) Quercetin reduces obesity-associated ATM in filtration and inflammation in mice: a mechanism including AMPK 1/SIRT1. *Journal of Lipid Research*, 55 (3): 363-374. https://doi.org/doi: 10.1194/jlr.M038786.

Draper, H.H., Hadley, M. (1990) Malondialdehyde determination as index of lipid peroxidation. *Methods in Enzymology*, 186: 421-31. https://doi.org/doi: 10.1016/0076-6879(90)86135-i

Etesami, B. Ghaseminezhad, S., Nowrouzi, A., Rashidipour, M and Yazdanparast, R.,2020. Investigation of 3T3-L1 cell differentiation to adipocyte, affected by aqueous seed extract of Phoenix Dactylifera L. *Reports Biochemistry and Molecular Biology,* 9(1): 14–25. https://doi.org/doi: 10.29252/rbmb.9.1.14.

Feng, A., Yang, S., Sun, Y., Zhangm L., Bo, F. Li, L. (2020) Development and evaluation of oleanolic acid dosage forms and its derivatives. *BioMed Research International*, 2020: 16. https://doi.org/10.1155-/2020/1308749.

Fernández-Poyatos, M.P., Ruiz-Medina, A., Zengin, G. Llorent-Martínez, E.J. (2019) Phenolic Characterization, Antioxidant Activity, and Enzyme Inhibitory Properties of Berberis thunbergii DC. Leaves: A Valuable Source of Phenolic Acids. *Molecules*, 24(22): 4171. https://doi.org/10.3390/molecules24224171.

Ghosh, J., Sil, P.C. (2013) Arjunolic acid: A new multifunctional therapeutic promise of alternative medicine. *Biochemistry and Molecular Biology*, 95(6): 1098-1109. https://doi.org/10.1016/j.biochi.2013.01.016.

Ginsberg, H.N., Packard, C.J., Chapman, M.J., Borén, J., guilar-Salinas, C.A.A., Averna, M., Ference, B.A., Gaudet, D., Hegele, R.A., Kersten, S. (2021) Triglyceride-rich lipoproteins and their remnants: metabolic insights, role in atherosclerotic cardiovascular disease, and emerging therapeutic strategies—a consensus statement from the European Atherosclerosis Society. *European Heart Journal*, 42(47): 4791–4806. https://doi.org/10.1093/eurheartj/ehab551.

Grati, W., Samet, S., Bouzayani, B., Ayachi, A., Treilhou, M., Téné, N., Jarraya, M.R. (2022) HESI-MS/MS analysis of phenolic compounds from *calendula aegyptiaca* fruits extracts and evaluation of their antioxidant activities. *Molecules*. 27(7): 2314. doi: 10.3390/molecules27072314.

Hassan, W.H.B., Abdelaziz, S., Al Yousef, H.M. (2018) Chemical composition and biological activities of the aqueous fraction of *parkinsonea aculeata* L. growing in saudi arabia. *Arabian Journal of Chemistry*, 12(3):377-387. https://doi.org/10.1016/j.arabjc.2018.08.003.

Hossain, M.K., Dayem, A.A., Han, J., Yin, Y., Kim, K., Saha, S.K., Yang, G.M., Yeon, C.H., Cho S.G. (2016) Molecular mechanisms of the anti-obesity and anti-diabetic properties of flavonoids. *International Journal of Molecular Sciences*, 17(4): 569. https://doi.org/doi: 10.3390/ijms17040569.

Ilavenil, S., Kim, D.H., Srigopalram, S., Arasu, M.V., Lee, K.D., Lee, J.C., Lee, J.S., Renganathan, S., Choi, K.C., (2016) Potential application of p-Coumaric acid on differentiation of C2C12 skeletal muscle and 3T3-L1 preadipocytes - an in Vitro and in Silico approach. *Molecules*, 21(8): 997. https://doi.org/10.3390/-molecules21080997.

Jakab, J., Miškić, B., Mikšić, Š., Juranić, B., Ćosić, V., Schwarz, D., Včev A. (2021) Adipogenesis as a potential anti-obesity target: a review of pharmacological treatment and natural products. *Diabetes Metabolic Syndrome*

Obesity: Targets and therapy, 8(14): 67—83. https://doi: 10.2147/DMSO.S281186.

Jang, G.H., Kim, H.W., Lee, M.K., Jeong, S.Y., Bak, A.R., Lee, D.J., Kim, J.B. (2018) Characterization and quantification of flavonoid glycosides in the Prunus genus by UPLC-DADQTOF/MS. *Saudi Journal of Biological Sciences*. 25(8): 1622-1631. https://doi.org/10.1016/j.sjbs.2016.08.001.

Jaradat, N., Zaid, A.N., Hussein, F., Zaqzouq M., Aljammal, H., Ayesh, O. (2017). Anti-Lipase Potential of the Organic and Aqueous Extracts of Ten Traditional Edible and Medicinal Plants in Palestine; a Comparison Study with Orlistat. Medicines (Basel), 4(4):89. https://doi.org/doi: 10.3390/medicines4040089.

Jung, U.J., Park, Y.B., Kim S.R., Choi, M.S. (2012) Supplementation of persimmon leaf ameliorates hyperglycemia, dyslipidemia and hepatic fat accumulation in type 2 diabetic mice. *PLOS One*. 7(11): e49030. https://doi.org/10.1371/journal.pone.0049030.

Kachlicki, P., Piasecka, A., Stobiecki, M., Marczak, Ł. (2016) Structural characterization of flavonoid glycoconjugates and their derivatives with mass spectrometric techniques. *Molecules*, 21(11):1494. https://doi.org/10.3390/molecules21111494

Karri, S., Sharma, S., Hatware, K., Patil, K. (2019) Natural anti-obesity agents and their therapeutic role in management of obesity: A future trend perspective. *Biomedicine & Pharmacotherapy*, 110 (1): 224–238. doi: 10.1016/j.biopha.2018.11.076.

Kerebba, N., Oyedeji, A.O., Byamukama, R., Kuria, S.K., Oyedeji O.O. (2022) UHPLC- UHPLC-ESI-QTOF-MS/MS characterisation of phenolic compounds from *Tithonia diversifolia* (Hemsl.) A. Gray and Antioxidant Activity. *Chemistry Select*, 7(16): e202104406-22. https://doi.org/10.1002/slct.202104406.

Khatua, B., El-Kurdi B., Singh, V.P. (2017) Obesity and pancreatitis. *Current Opinion in Gastroenterology*, 33(5): 374–382. doi: 10.1097/MOG.0000000000000386.

Kim, B.M., Cho, B.O., Jang, S.I. (2019) Anti-obesity effects of *Diospyros lotus* leaf extract in mice with high-fat diet-induced obesity. *International Journal of Molecular Medicine*, 43(1):603-613. DOI: 10.3892/ijmm. -2018.3941.

Konige, M., Wang, H., Sztalryd, C. (2013) Role of adipose specific lipid droplet proteins in maintaining whole body energy homeostasis. *Biochimica et Biophysica Acta*, 1842 (3):393-401. doi: 10.1016/j.bbadis.2013.05.007.

Kraus, N.A., Ehebauer, F., Zapp, B., Rudolphi, B., Kraus, B.J., Kraus, D. (2016) Quantitative assessment of adipocyte differentiation in cell culture. *Adipocyte*, 5(4): 351–358. doi: 10.1080/21623945.-2016.1240137.

Kumar, S., Pandey, A.K. (2013) Chemistry and biological activities of flavonoids: an overview. *Scientific World Journal*, 2013: 162750. doi: 10.1155/2013/162750

Lewis, D.R., Liu, D.G, 2012. Direct measurement of lipase inhibition by orlistat using a dissolution linked in vitro assay. *Clinical Pharmacology & Biopharmaceutics*, 1(3):1–3. https://doi.org/10.4172/2167-065X.1000-103.

Li, M., Pu, Y., Yoo, C.G., Ragauskas, A.J. (2016) The occurrence of tricin and its derivatives in plants. *Green Chemistry*, 18(6):1439-1454. https://doi.org/10.1039/c5gc03062e.

Lin, KW., Huang, A.M., Tu, H.Y., Weng, J.R., Hour, T.C., Wei, B.L., Yang, S.C., Wang, J.P., Pu, Y.S., Lin, C.N., (2009) Phloroglucinols inhibit chemical mediators and xanthine oxidase, and protect cisplatin-induced cell death by reducing reactive oxygen species in normal human urothelial and bladder cancer cells. *Journal of Agricultural and Food Chemistry*. 57 (19): 8782–8787. https://doi.org/10.1021/jf900935n

Liu, N., Liu, Y., Dong, D., Yu, J., Yuan, H. (2022) Effects of inflammatory factor expression regulated by 12/15 lipoxygenase on obesity-related nephropathy. *Nutrients*, 14(13): 2743. https://doi.org/doi: 10.3390/-nu14132743

Llorent-Martínez, E.J., Gouveiaa, S., Castilhoa, P.C. (2015) Analysis of phenolic compounds in leaves from endemic trees from Madeira Island. A contribution to the chemotaxonomy of Laurisilva forest species. *Industrial Crops and Products*, 64:135-151. https://doi.org/10.1016/j.indcrop.2014.10.068

Lloyd-Jones, D.M., Morris, P.B., Ballantyne, C.M., Birtcher, K.K., Covington, A.M., De Palma, S.M., Minissian, M.B., Orringer, C.E., Smith, J.S.C., Arana, W,A., John, T.W. (2022) ACC Expert consensus decision pathway on the role of Nonstatin therapies for ldl-cholesterol lowering in the management of atherosclerotic cardiovascular disease risk: a report of the American college of cardiology solution set oversight committee writing committee. *Journal of the American College of Cardiology*, 4;80 (14):1366-1418. https://doi.org/doi: 10.1016/j.jacc.2022.07.006.

Lourenço, A., Marques, A.V., Gominho, J. (2021) The identification of new triterpenoids in eucalyptus globulus wood. *Molecules*, 26(12):3495-3508. https://doi.org/10.3390/ Molecules-26123495.

Mahboob, A., Samuel, S.M., Mohamed, A., Wani, M.Y., Ghorbel, S., Miled, N., Büsselber D., Chaari A. (2023) Role of flavonoids in controlling obesity: molecular targets and mechanisms. *Frontiers in Nutrition*, (10): 1177897. https://doi.org/10.3389/fnut.2023.1177897.

Manna, P. (2015) Obesity, oxidative stress, adipose tissue dysfunction, and the associated health risks: causes and therapeutic and therapeutic strategies. *Metabolic Syndrome and Related Disorders*, 13(10): 423–444. https://doi.org/10.1089/met.2015.0095.

Miller, L., Thompson, K., Pavlenco, C., Mettu, V.S., Haverkamp, H., Skaufel, S., Basit, A., Prasad, B., Larsen, J. (2021) The effect of daily methylsulfonylmethane (MSM) consumption on high-density lipoprotein cholesterol in healthy overweight and obese adults: A randomized controlled trial. *Nutrients*, 13(10): 3620. https://doi.org/doi: 10.3390/nu13103620.

Mohsen, G.A.M., Abu-Taweel, G.M., Rajagopal, R.; Sun-Juc, K., Kimd H.J., Kimc, Y.O., Mothana, R.A., Kadaikunnan, S., Jamal, M.K., Siddiqui, N.A., Al-Rehaily, A.J. (2019) Betulinic acid lowers lipid accumulation in adipocytes. *The Journal of Infection and Public Health*. 12 (5): 726-732. https://doi.org-/10.1016/j.jiph.2019.05.011

Mubtasim, N., Gollahon, L. (2023) Characterizing 3T3-L1 MBX adipocyte cell differentiation maintained with fatty acids as an in vitro model to study the effects of obesity. *Life (Basel)*, 13(8):1712- 1740. https://doi.org/10.3390/life13081712.

Mutai, C., Abatis, D., Vagias, C., Moreau, D.; Roussakis, C., Roussis, V. (2007) Lupane triterpenoids from *acacia mellifera* with cytotoxic activity. *Molecules*, 12(5): 1035-1044. doi: 10.3390/12051035.

Nandi, A., Yan, L., Jana, C.K., Das, N. (2019) Role of Catalase in Oxidative Stress- and Age-Associated Degenerative Diseases, *Oxidative Medicine and Cellular Longevity*, 2019:19 pages. https://doi.org/-10.1155/2019/9613090.

Ngoc, H.N., Tran, C.A., Trinh, T.D., Thi, N.L.N., Phan, H.N.T., Le, V.N., Le, N.H., Phung, V. T. (2022) UHPLC-Q-TOF-MS/MS dereplication to identify chemical constituents of *Hedera helix* leaves in vietnam. *Journal of Analytical Methods in Chemistry*, (1):1-18. https://doi: 10.1155/2022/1167265. eCollection.

Nguyen, H.T., Pandey, R.P., Thuy T.T.T., Park J.W., Sohng, J.K. (2013) Improvement of regio-specific production of myricetin-3-o-α-l-rhamnoside in engineered Escherichia coli. *Biotechnology and Applied Biochemistry*, 171(8):1956-67. https://doi.org/10.1007/s12010-013-0459-9.

Oboh, M., Govender, L., Siwela, M., Mkhwanazi, B.N. (2021) Anti-diabetic potential of plant-based pentacyclic triterpenes derivatives: progress made to improve efficacy and bioavailability. *Molecules*, 26 (23): 7243. https://doi.org/10.3390/molecules26237243.

Okba, M.M., El - Shiekh, R.A., Abu-Elghait, M., Sobeh, M., Ashour, R.M.S. (2021) HPLC-PDA-ESI-MS/MS profiling and anti-Biofilm potential of *Eucalyptus sideroxylon* Flowers. *Antibiotics*. 10(7):761-778. https://doi: 10.3390/antibiotics10070761.

Pacher, P., Beckman, J.S., Liaudet L. (2007). Nitric oxide and peroxynitrite in health and disease. *Physiological Reviews*, 87(1):315-424. https://doi: 10.1152/physrev.00029.2006.

Pereira, P., Cebola, M., Oliveira, M., C., Gil, M.G.B. (2017) Antioxidant capacity and identification of bioactive compounds of *Myrtus communis* L. extract obtained by ultrasound-assisted extraction. *The Journal of Food Science and Technology*, 54(13):4362-4369. https://doi: 10.1007/s13197-017-2907-y.

Prieto, P., Pineda M., Aguilar, M. (1999) Spectrophotometric Quantitation of Antioxidant Capacity through the Formation of a Phosphomolybdenum Complex: Specific Application to the Determination of Vitamin E. *Analytical Biochemistry*, 269 (2): 337-341. https://doi.org/10.1006/abio.1999.4019.

Rached, W., Bnnaceur, M., Barros, L., Calhelha, R.C., Heleno, S., Alves, M.J., Carvalho, A.M. Maroufe, A., Ferreira, I.C. F. R. (2017) Detailed phytochemical characterization and bioactive properties of *Myrtus nivelii* Batt & Trab. *The Royal Society of Chemistry*, 9 (8): 3111–3119. https://doi.org/10.1039/C7FO00-744B.

Rahmati, A.S., Broom, D.R., Ghanbari-Niaki, A., Shirvani, H. (2019) Effects of exercise on reverse cholesterol transport: A systemized narrative review of animal studies. *Life Sciences,* 1(224):139-148. https://doi: 10.1016/j.lfs.2019.03.058.

Razgonova, M., Zakharenko, A., Pikula, K., Manakov, Y., Ercisli, S., Derbush, I., Kislin, E., Seryodkin, I., Sabitov, A., Kalenik, T., Golokhvast, K., 2021. LC-MS/MS screening of phenolic compounds in wild and cultivated *Grapes Vitis* amurensis rupr. *Molecules*, 26(12): 3650- 55. https://doi: 10.3390/molecules26123650.

Sabatine, M.S., Giugliano, R.P., Keech, A.C., Honarpour, N., Wiviott, S.D., Murphy, S.A., Kuder, J.F., Wang, H., Liu, T., Wasserman, S.M., Sever, S.P., Pedersen, T.R. (2017) Evolocumab and clinical outcomes in patients with cardiovascular disease. *The New England journal of medicine*, 4;376 (18):1713-1722. https://doi.org/ doi: 10.1056/NEJMoa1615664.

Saldanha, L.L., Vilegas, W., Dokkedal, A.L. (2013) Characterization of flavonoids and phenolic acids in *Myrcia bella Cambess*. using FIA-ESI-IT-MS and HPLC-PAD-ESI-IT-MS combined with NMR. *Molecules*, 18(7): 8402–8416. https://doi.org/ 10.3390/molecules18078402.

Shi, J., Gao, X., Zhang, A., Qin, X., Du, G. (2022) Characterization of multiple chemical components of GuiLing Ji by UHPLC-MS and 1 H NMR analysis. *Pharmaceutical Analysis*, 12 (3): 460-469. https://doi.org/10.1016-/j.jpha.2021.09.013

Singh, A., Bajpaia, V., Kumara, S., Sharma, K.R, Kumara, B. (2016) Profiling of gallic and ellagic acid derivatives in different plant parts of *Terminalia arjuna* by HPLC-ESI-QTOF-MS/MS. *Natural Product Communications*, 11 (2): 239 – 244. https://doi.org/10.1177/1934578X1601100227

Sliwka-Kaszynska, M., Anusiewicz, I., Skurski, P. (2022) The mechanism of a retro-diels–alder fragmentation of luteolin: theoretical studies supported by electrospray ionization tandem mass spectrometry results. *Molecules*, 27(3): 1032-1048. https://doi.org/10.3390/molecules27031032.

Su, H., Feng, L., Zheng, X., Chen, W. (2016) Myricetin protects against diet-induced obesity and ameliorates

oxidative stress in C57BL/6 mice. *Journal of Zhejiang University Science B*, 17(6):437-.46. https://doi.org/10.1631/jzus. B1600074.

Tanaka, M.; Sugama, A.; Sumi, K.; Shimizu, K.; Kishimoto, Y.; Kondo, K., Iida, K. (2020) Gallic acid regulates adipocyte hypertrophy and suppresses inflammatory gene expression induced by the paracrine interaction between adipocytes and macrophages in vitro and in vivo. *Nutrition Research*, 73:58-66. https://doi.org/doi: 10.1016/j.nutres.2019.09.007.

Taye, A.D., Bizuneh, G.K., Kasahun, A.E. (2023) Ethnobotanical uses, phytochemistry and biological activity of the genus Euclea. *A review. Frontiers Pharmacology*, 14: 1170145. https://doi.org/10.3389/fphar.2023-.1170145

Thuan, H.N., Pandey, R.P., Thuy, T.T.T., Park, J.W., Sohng, J.K. (2013) Improvement of regio-specific production of myricetin-3-o-α-l-rhamnoside in engineered *Escherichia coli*. *Applied Biochemistry and Biotechnology* 171(8): 1956–1967. https://doi.org/10.1007/s12010-013-0459-9.

Van, R.L.R., Roncari, D.A.K. (1977) Isolation of fat cell precursors from adult rat adipose tissue. *Cell Tissue Research*, 181, 197–203. https://doi.org/10.1007/BF00219980.

Xia, B., Bai, L., Li, X., Xiong, J., Xu, P.M., Xue, M. (2015) Structural analysis of metabolites of asiatic acid and its analogue madecassic acid in Zebrafish using LC/IT-MSn. *Molecules*, 20(2):3001-19. https://doi.-org/10.3390/molecules20023001.

Xiang, L., Liu, M., Xiang, G., Ling, Y., Zhang, J., Xu, X., Dong, J. (2024) Dapagliflozin promotes white adipose tissue browning though regulating angiogenesis in high fat induced obese mice. *BMC Pharmacology and Toxicology*, 25:26. https://doi.org/10.1186/s40360-024-00747-5.

Xie, L., Deng, Z., Zhang, J., Dong, H., Wang, W., Xing, B., Liu, X. (2022) Comparison of flavonoid o-glycoside, c-glycoside and their aglycones on antioxidant capacity and metabolism during in vitro digestion and in vivo. *Foods*, 11(6): 882. doi: 10.3390/foods11060882.

Yan, S.L., Yang, H.T., Lee, Y.J., Lin, C.C., Chang, M.H., Yin, M.C. (2014) Asiatic acid ameliorates hepatic lipid accumulation and insulin resistance in mice consuming high fat diet. *Journal of Agricultural and Food Chemistry*, 62 (20). https://doi.org/10.1021/jf501165z.

Yang, Y.Y., Qi, J.J., Jiang, S.Y., Ye, L. (2024) Esculin ameliorates obesity-induced insulin resistance by improving adipose tissue remodeling and activating the IRS1/PI3K/AKT/GLUT4 pathway. *Ethnopharmacology*, p. 117251 . https://doi.org/10.1016/j.jep.2023.117251.

Yen, G.C., Cheng, H.L., Lin, L.Y., Chen, S.C., Hsu, C.L. (2020) The potential role of phenolic compounds on modulating gut microbiota in obesity. *Journal of Food and Drug Analysis,* 28(2): 195–205. https://doi.org/-10.38212/2224-6614.1054.

Yunusoglu, O., Türkmen, Ö., Berkoz, M., Yıldırım, M., Yalın, S. (2022) In vitro anti-obesity effect of *Aloe vera* extract through transcription factors and lipolysis associated genes. *Eastern Journal of Medicine*, 27(4): 519-528. https://doi.org/10.5505/ejm.2022.13285.

Zhang, X., Li, X., Fang, H., Guo, F., Li, F., Chen, A., Huang, S. (2019) Flavonoids as inducers of white adipose tissue browning and thermogenesis: Signaling pathways and molecular triggers. *Nutrition & Metabolism*, 16: 47. https://doi.org/doi: 10.1186/s12986-019-0370-7.